CANCER

Exploiting evolutionary principles to prolong tumor control in preclinical models of breast cancer

Pedro M. Enriquez-Navas,[1] Yoonseok Kam,[1] Tuhin Das,[1] Sabrina Hassan,[1] Ariosto Silva,[1] Parastou Foroutan,[1]* Epifanio Ruiz,[1] Gary Martinez,[1,2] Susan Minton,[3] Robert J. Gillies,[1,4] Robert A. Gatenby[1,4]†

Conventional cancer treatment strategies assume that maximum patient benefit is achieved through maximum killing of tumor cells. However, by eliminating the therapy-sensitive population, this strategy accelerates emergence of resistant clones that proliferate unopposed by competitors—an evolutionary phenomenon termed "competitive release." We present an evolution-guided treatment strategy designed to maintain a stable population of chemosensitive cells that limit proliferation of resistant clones by exploiting the fitness cost of the resistant phenotype. We treated MDA-MB-231/luc triple-negative and MCF7 estrogen receptor–positive (ER$^+$) breast cancers growing orthotopically in a mouse mammary fat pad with paclitaxel, using algorithms linked to tumor response monitored by magnetic resonance imaging. We found that initial control required more intensive therapy with regular application of drug to deflect the exponential tumor growth curve onto a plateau. Dose-skipping algorithms during this phase were less successful than variable dosing algorithms. However, once initial tumor control was achieved, it was maintained with progressively smaller drug doses. In 60 to 80% of animals, continued decline in tumor size permitted intervals as long as several weeks in which no treatment was necessary. Magnetic resonance images and histological analysis of tumors controlled by adaptive therapy demonstrated increased vascular density and less necrosis, suggesting that vascular normalization resulting from enforced stabilization of tumor volume may contribute to ongoing tumor control with lower drug doses. Our study demonstrates that an evolution-based therapeutic strategy using an available chemotherapeutic drug and conventional clinical imaging can prolong the progression-free survival in different preclinical models of breast cancer.

INTRODUCTION

Chemotherapy with cytotoxic drugs is widely used for breast cancer treatment in neoadjuvant, adjuvant, and metastatic clinical settings (*1*). In general, cytotoxic drugs are administered with the assumption that maximum clinical benefit is obtained by killing the greatest possible number of cancer cells. Consistent with this premise, most systemic cancer chemotherapies are applied at the maximum tolerated dose density (*3*–*5*), which has the theoretical benefits of killing the largest number of cancer cells and minimizing the risk of resistant mutations. Metronomic therapy has been investigated as an alternative strategy that uses lower drug doses administered more frequently (*6*, *7*). Although it is qualitatively different, this approach maintains the same basic intent of maximum tumor cell death through greater cumulative doses and antiangiogenic effects (*8*).

Recently, the traditional maximum dose density paradigm has been questioned (*9*, *10*) on the basis of a theoretical model that views cancer therapy as an evolutionary and ecological process. This alternative model rests on three major assumptions: First, phenotypically or environmentally mediated resistant cells are present before treatment (*11*, *12*). Second, most xenobiotic mechanisms protecting cells from cytotoxic agents do not require mutations, but rather increased expression of molecular machinery already encoded in the genome (*13*). Third, cancer populations within a tumor compete with each other for space and substrate (*14*, *15*).

Clearly, in the presence of chemotherapy, resistant cells are better adapted and, thus, fitter (more proliferative) than wild-type cells. However, in the absence of chemotherapy, this fitness difference is typically reversed because of the metabolic cost of the resistance mechanism (synthesis, maintenance, and operation of membrane extrusion pumps). For example, cells expressing the multidrug resistance (MDR) phenotype can expend up to one-third of their total ATP (adenosine 5′-triphosphate) production for operation of the associated membrane pumps (*16*). In an environment of limited substrate, this cost requires diversion of resources from proliferation and invasion. The evolutionary consequences of this trade-off are demonstrated by observations that P-glycoprotein–expressing cells (MCF7-dox) revert to wild type unless doxorubicin is maintained in the culture media as a strong selection force (*17*). In this Darwinian setting, maximum dose density therapy strongly selects for resistant phenotypes and, by removing all competitors, permits unconstrained proliferation of the resistant populations even when no drug is present—a phenomenon well recognized in evolutionary dynamics as "competitive release" (*18*, *19*).

Here, we investigate an alternative, evolution-based treatment strategy (*10*, *20*–*23*) that aims to maximize time to progression rather than reduction in tumor size. This approach applies limited, short bursts of therapy with an explicit goal of maintaining a residual population of treatment-sensitive cells. When therapy is withdrawn, this population suppresses proliferation of resistant tumor cells because of its fitness advantage in the absence of drug.

In earlier work (*10*, *23*), we framed this treatment strategy mathematically and presented supportive in vitro and in vivo experimental evidence in ovarian cancer. An unanticipated observation in the initial

[1]Department of Cancer Imaging and Metabolism, H. Lee Moffitt Cancer Center and Research Institute, Tampa, FL 33612, USA. [2]Department of Physics, University of South Florida, Tampa, FL 33620, USA. [3]Department of Women's Oncology, H. Lee Moffitt Cancer Center and Research Institute, Tampa, FL 33612, USA. [4]Cancer Biology and Evolution Program, H. Lee Moffitt Cancer Center and Research Institute, Tampa, FL 33612, USA.
*Present address: Bruker BioSpin Corp., Billerica, MA 01821, USA.
†Corresponding author. E-mail: robert.gatenby@moffitt.org

Downloaded from http://stm.sciencemag.org/ at UNIVERSITY OF NORTH TEXAS on December 18, 2020

in vivo studies with ovarian cancer was that, once tumor control was achieved, it could be maintained with progressively lower doses of the chemotherapy agent (*23*).

Here, we address four questions that arose from these investigations. First, can adaptive therapy (AT) be applied to other cancer types? Second, what is the optimal strategy for adaptively maintaining a stable tumor: regular application of decreasing doses of drug or skipping doses when the tumor is stable? Third, can routine clinical imaging [for example, magnetic resonance imaging (MRI)] provide sufficient information on tumor size to guide therapy? Fourth, what is the mechanism for increased drug efficacy once initial control is achieved?

Here, we applied AT to MDA-MB-231/luc, a metastatic triple-negative human breast cancer cell line, and to MCF7, a less aggressive ER^+ human breast cancer cell line, orthotopically implanted in the mouse mammary fat pad and treated with paclitaxel. We used MRI scans to measure the tumor volume and, consequently, guide the therapeutic algorithms. To optimize the AT algorithm, we examined the control achieved by continuous dose adjustment versus skipping treatment doses. Finally, we performed both diffusion-weighted (DW) and dynamic contrast-enhanced MRI of the tumors during therapy to assess changes in tumor vascularity and blood flow during enforced stabilization of the tumor volume compared to progressive growth. We used these in vivo studies along with histological examination of the tumors at the completion of the experiment to examine our hypothesis that the progressively lower doses necessary for tumor control in the initial AT experiments were the result of vascular normalization that may both limit invasive tumor growth and maximize drug delivery (*24*–*26*).

RESULTS

Tumor growth control by AT

We evaluated the responses of MDA-MB-231 tumors to three different therapies: conventional maximum dose density application of paclitaxel (ST), AT in which the frequency of dosing is maintained but with decreasing doses as the tumor responds (AT-1), and AT in which doses of paclitaxel are never lowered but rather doses are skipped when the tumor is responding (AT-2). Additional details can be found in Materials and Methods and fig. S1. First, we compared the treatment outcome of ST with AT-1. In Fig. 1A, both ST and AT-1 treatments suppressed tumor growth successfully for the initial period (10 to 20 days). However, tumor growth in the ST group rapidly recovered after the scheduled treatment was over. In contrast, the tumor burden remained stable relative to the initial tumor volume for a longer period under AT-1 than under ST, similarly to the previous AT trials in an ovarian cancer model (*8*). We applied the same treatment algorithms to larger tumors and observed that AT-1 produced a long-term stabilization of tumor burden (Fig. 1B). In both trials, nearly all of the tumors in the AT-1 group (six of seven mice) reached the minimum tumor volume cutoff for being treated (see AT-1 description in Materials and Methods), and remained small and stable throughout the prolonged follow-up period, requiring lower and lower doses of chemotherapy and eventually allowing treatment withdrawal.

Because frequent administration of chemotherapy is challenging in clinics, we investigated a dose-skipping algorithm (AT-2) in which tumors that were stable between measurements received no therapy rather than an adjusted (lower) dose, as dictated by the algorithm for AT-1. In Fig. 1C, ST initially reduced tumor volume but usually was not curative, and the tumors recurred. AT with dose skipping (AT-2) controlled tumor volume for a longer period. However, unlike the results in AT-1, the tumors generally progressed through the AT-2 strategy.

To obtain a more precise comparison between these two AT algorithms, we applied both AT treatment methods in the same batch of animals. In Fig. 1D, AT-1 controlled the tumor growth better than AT-2 in all cases. As in trials 1 and 2, 66% (four of six mice) of the tumors treated according to AT-1 ultimately became stable even when therapy was withdrawn.

To ensure that our findings were generalizable to different cancer types, we injected other cohorts of mice with MCF7 cells (Fig. 2), an estrogen receptor–positive (ER^+) slowly invasive human breast cancer. In this case, because the cell line is estrogen-dependent (ER^+), we had to implant estrogen pellets (0.72 mg of β-estradiol, slow release) in the animals before injecting the tumor cells. The same therapies were applied to this cohort, showing that AT-1 maintained a stable tumor volume for extended periods in all cases. Similar to the earlier experiments,

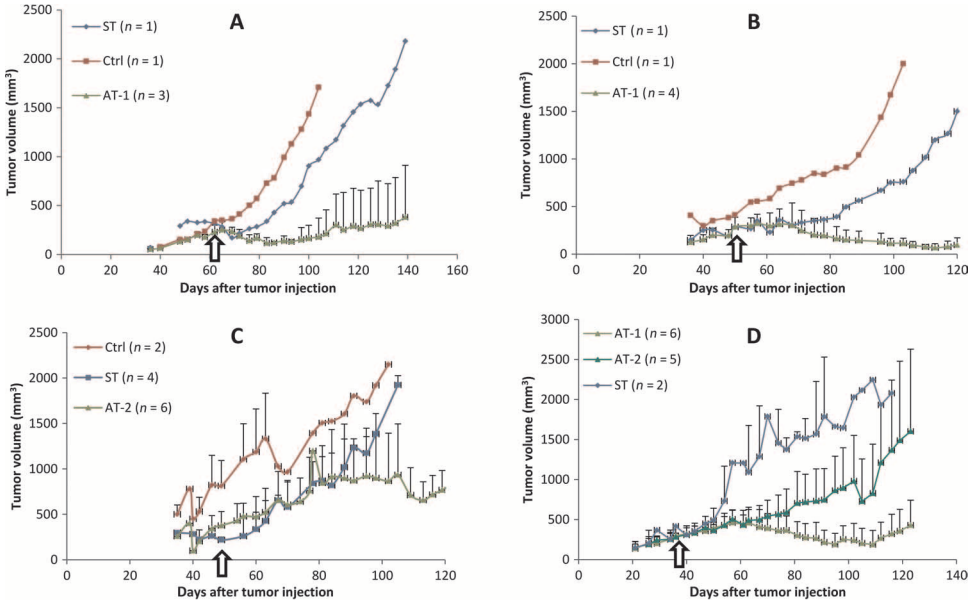

Fig. 1. MRI volumetric data for the different treatments applied to MDA-MB-231 preclinical models. (**A** to **D**) Different cohorts of mice injected at different times. Control (Ctrl) animals did not receive any chemotherapy. The mice in the ST group received the standard high-dose treatment [paclitaxel, 20 mg/kg intraperitoneally, twice a week for 2.5 weeks]. AT groups received different doses depending on the algorithm (AT-1 or AT-2; see Materials and Methods). Data are means ± SD. More detailed results, including ADC values and volumes for individual tumors, are available in fig. S1. Arrows indicate when the treatment in the ST group was stopped.

Downloaded from http://stm.sciencemag.org/ at UNIVERSITY OF NORTH TEXAS on December 18, 2020

therapy was ultimately withdrawn in three of the five (60%) mice with no further progression. Also similar to the earlier experiments, we found that the AT-2 strategy did not maintain a stable tumor volume.

Prolonged survival benefit of AT with dose adjustments

To corroborate the progression-free survival benefits of AT, we analyzed the therapy outcomes by Kaplan-Meier estimation. We counted the number of mice with tumor size under 1000 mm^3, assuming this as a lethal tumor burden, and plotted them as shown in Fig. 3. In the case of MDA-MB-231 (Fig. 3A), all mice in the control group reached the tumor volume limit of 1000 mm^3 with a median progression-free survival of 75.5 days. Administration of high-dose paclitaxel (ST) resulted in a rapid decline of tumor volume followed by rapid progression. In two animals in this cohort, the initial high-dose regimen was reinstituted after progression but had no effect on tumor growth, indicating that a highly resistant phenotype had been selected by the initial dose. ST and AT-2 delayed the progression at medians of 108.5 and 109 days, respectively. In both of these treatment cohorts, most of the mice developed tumors larger than the limit by ~100 days after injection, and the survival benefit was not significant ($P = 0.3835$ and 0.1573, respectively). Although AT-2 appeared to have a better treatment outcome than ST in Fig. 1, there was no significant benefit in progression-free survival ($P = 0.9163$). In contrast, AT-1 achieved a significant survival benefit ($P = 0.0006$), with only 2 of the 12 (16%) animals progressing beyond 1000 mm^3 tumor burden within the 155 days of these trials.

Figure 3B demonstrates the results in MCF7 mice. In control, ST, and AT-2, all the mice reached a tumor volume larger than 1000 mm^3 during the monitoring time. However, only one of the AT-1 animals reached this limit during the same period of time, indicating a significant survival benefit ($P = 0.03$). There was no significant survival benefit in any of the other three groups.

Figure 4 and fig. S2 show the total dose of drug administered using the three different treatment strategies. Because the animals lived longer, the cumulative doses in the AT-1 group exceeded those for both AT-2 and ST in both cell lines. This higher total dose also reflected our findings that stabilizing the volume of an initially exponentially growing tumor required aggressive initial therapy with total drug doses greater than those of ST but given over a longer time period. However, once control of the tumor was obtained, the doses could be rapidly reduced and even withdrawn (fig. S3) so that the slopes of drug dose accumulation in AT-1 mice decreased over time in Fig. 4 and fig. S2. None of the mice in any of the treatment groups showed evidence of toxicity, maintaining a stable body weight (tables S1 to S4).

MRI analysis and assessment of treatment response

DW MRI images with different *b* values (that is, with different strength of diffusion-sensitizing factor) were acquired and analyzed to generate apparent diffusion coefficient (ADC) maps of the tumors. Because ADC is highest in areas of cytotoxic or vasogenic edema and necrosis, we used these maps to estimate the percentage of necrotic tissue during tumor monitoring.

In Fig. 5, MDA-MB-231 AT-2– and ST-treated tumors developed increasing tumor necrosis over time. The AT-1 cohort exhibited a generally decreasing amount of necrosis over time (after an initial increase). In the MCF7 mice, AT-1 therapy maintained a stable volume fraction of necrosis throughout treatment, whereas it generally increased in the other cohorts.

In Fig. 6, we show that dynamic contrast enhancement (DCE) MRI imaging before, during, and after therapy demonstrated greater blood flow in the tumors treated with AT-1 in both cell lines.

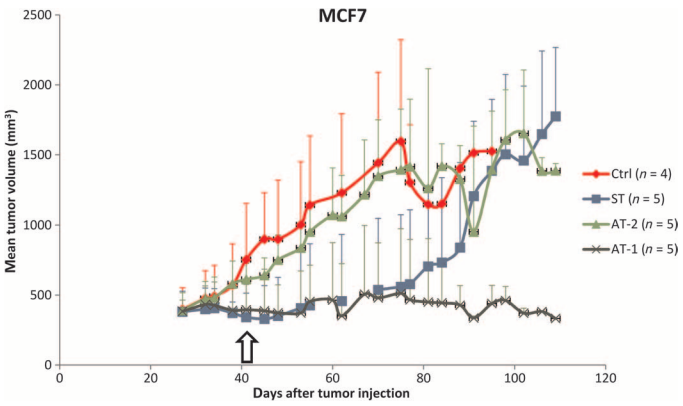

Fig. 2. MRI volumetric data for the different treatments applied to MCF7 preclinical models. Ctrl animals did not receive any chemotherapy. The mice in the ST group received the standard high-dose treatment (paclitaxel, 20 mg/kg intraperitoneally, twice a week for 2.5 weeks). AT groups received different doses depending on the algorithm (AT-1 or AT-2; see Materials and Methods). Data are means ± SD. More detailed results, including ADC values and volumes for individual tumors, are available in fig. S1. Arrow indicates when the treatment was stopped in the ST mice.

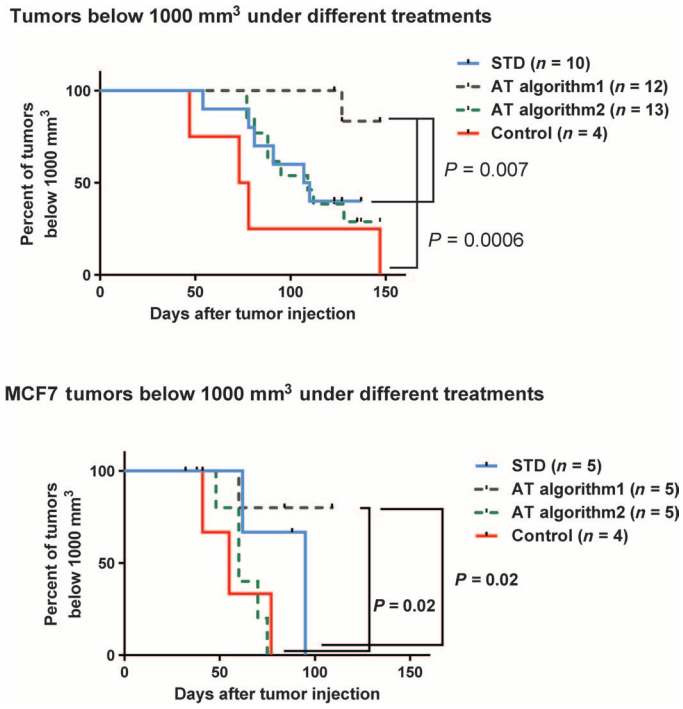

Fig. 3. Survival of animals treated by different therapeutic algorithms. The Kaplan-Meier plots show animals with tumor volumes smaller than 1000 mm^3 after treatment according to the standard (STD) or adaptive (AT-1 and AT-2) strategies. In the legend, *n* corresponds to the number of animals under each treatment algorithm. (**A** and **B**) Mice injected with MDA-MB-231 (A) and MCF7 (B) cell lines. Statistics were calculated with the Mantel-Cox test.

Downloaded from http://stm.sciencemag.org/ at UNIVERSITY OF NORTH TEXAS on December 18, 2020

Histological examination

At the completion of monitoring, we performed immunohistochemistry (IHC) including hematoxylin and eosin (H&E), CD31, and smooth muscle actin (SMA) staining of each tumor to calculate necrotic and viable tumor volumes, vascularity density, and integrity of the vessels, respectively. All of the tumors were fully occupied by cancer cells that were morphologically identical to the parental cell line, even in those animal in which tumor remained controlled after therapy was withdrawn.

In Fig. 7 (top row), we demonstrate that the necrotic fraction of MDA-MB-231 tumors under AT-1 was the smallest among the tested therapies. Also, the in vivo change in necrosis calculated by ADC maps from DW MRI experiments (Fig. 5) showed that AT-1 maintained the amount of necrosis at a more stable level than the other therapies tested.

Consistent with these results and the DCE MRI experiments, CD31 staining (Fig. 7) demonstrated that vascular density was highest in the AT-1 cohort. SMA staining showed that the vascular walls were not statistically different among the groups.

Histological examination of the MCF7 tumors showed only low amounts of necrosis, which were not significantly different among the cohorts (Fig. 7). However, CD31 staining showed a higher mean vascular density in the AT-1 and AT-2 (the latter being significantly different, $P = 0.04$) compared to the ST and control groups. In contrast, SMA (measured to assess vessel functionality) staining was significantly increased ($P \leq 0.002$) in AT-1 compared to the rest of the treatments.

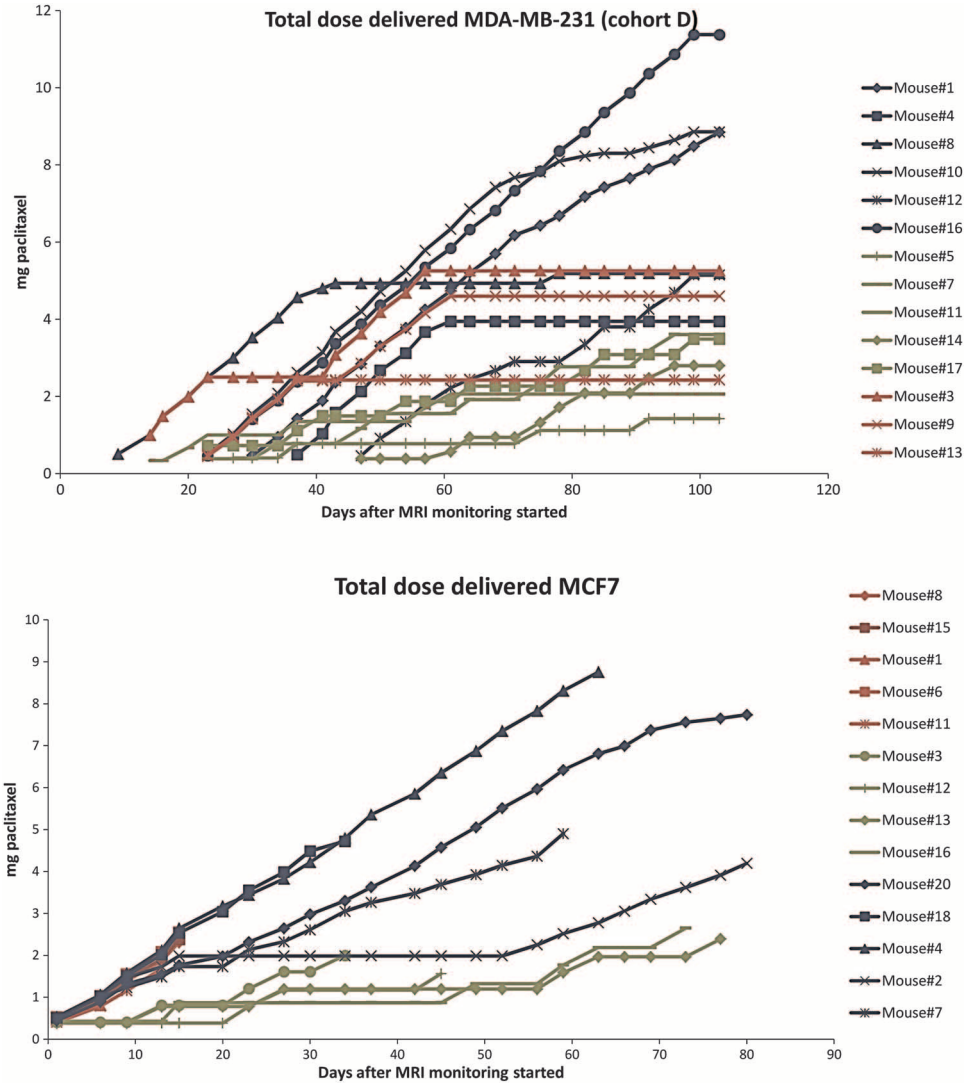

Fig. 4. Total delivered dose of paclitaxel with each algorithm. Total delivered dose of paclitaxel for MDA-MB-231 cohort D (upper graph) and MCF7 cohort (lower graph) is shown as the cumulative dose of paclitaxel for each day after MRI monitoring had started. Blue corresponds to mice treated under AT-1; green, mice treated under AT-2; and red, animals under ST treatment. Note that mouse#9 and mouse#13 in the MDA-MB-231 group received two sessions of ST therapy to demonstrate that the cancer cells that recur after standard therapy are drug-resistant. Cumulative dose graphs for MDA-MB-231 cohorts A to C are shown in fig. S2.

DISCUSSION

The emergence and proliferation of drug-resistant phenotypes in advanced and metastatic cancers result in treatment failure and disease progression. We propose that this process is governed by Darwinian principles and that conventional maximum dose density chemotherapy accelerates the evolutionary dynamics that permit unopposed proliferation of resistant tumor populations—a phenomenon known as competitive release.

In previous investigations, we applied computational methods from this evolutionary model to develop therapeutic strategies that exploit Darwinian dynamics to prolong response to therapy and delay proliferation of resistant populations (*23*). This approach requires the dynamic adjustment of drug dose and timing on the basis of tumor response, to maintain a balance between chemoresistant and chemosensitive cells so that the latter can suppress the proliferation of the former. This approach was initially framed mathematically and then applied successfully to ovarian cancer xenografts (OVCAR) treated with carboplatin (*23*). Because the evolutionary dynamics of tumors are tightly linked to the microenvironment, we examined AT in triple-negative (MDA-MB-231) and ER^+ (MCF7) breast cancers growing orthotopically in the mammary fat pad of female mice. The MDA-MB-231 cell line has been studied extensively and is heterogeneous at the tissue and cellular levels, typically consisting of a mixture of resistant and sensitive populations (*11*, *27*–*30*). The MCF7 cell line, typical of ER^+ tumors, is generally slower-growing, is weakly invasive, and forms fewer metastases when compared to the MDA-MB-231

Downloaded from http://stm.sciencemag.org/ at UNIVERSITY OF NORTH TEXAS on December 18, 2020

line (*31*). A number of mechanisms for resistance to paclitaxel have been found in cancers, but an increase in xenobiotic metabolism is most commonly observed in resistant MDA-MB-231 and MCF7 cell lines (*32*).

Because the application of evolutionary principles is based on previous responses to therapy, successful treatment requires continuous, accurate measurement of tumor volume or, more ideally, the mass of viable tumor cells. In clinical trials, most tumor measurements are performed with cross-sectional imaging. For this reason, we based our treatment algorithms on tumor volume measured by MRI.

Our results demonstrated that conventional high-dose standard therapy (ST) could markedly reduce the tumor burden, but complete eradication was rare. Unlike ST therapy, in which the dose of therapy was fixed and the tumor size was the outcome variable, AT attempts to fix the tumor size by constantly adjusting drug dosing. Ideally, this variation in therapy would include both different drugs and doses. Here, however, for simplicity, we used only paclitaxel and adjusted its dose to maintain a constant tumor size.

In general, we observed that application of AT is a two-phase process. In an induction phase, the exponential growth of the untreated tumor must be forced to plateau. In the second phase, once tumor control is established, it must be maintained. We find that successful control of tumor in each phase requires a different strategy.

In MDA-MB-231 tumors, gaining control of the exponentially growing tumor proved to be challenging. In control animals, the tumor typically doubled in volume in 20 days. High-dose density therapy often markedly reduced the tumor size, but cure was rare. We attempted to use a dose-skipping (AT-2) approach, reasoning that less frequent treatment could more readily be applied to a clinical setting. However, this was almost always unsuccessful because the tumor frequently grew uncontrollably during even a single skipped dose. In contrast, we found that application of therapy with consistent frequency but lowered doses (AT-1) according to response consistently achieved tumor control. Nearly identical results were obtained in the initial therapy for the less-aggressive, ER^+ cell line.

The dynamics governing this critical first phase of AT will require additional investigation. The AT-1 algorithm permitted a higher cumulative drug dose, so it appears that treatment intensity as well as timing may be critical factors for gaining initial tumor control. However, other issues such as tumor angiogenesis, blood flow, and immune response are likely to affect outcomes.

In the second phase of therapy, we found that maintaining both MDA-MB-231 and MCF7 tumors at their plateau could be achieved fairly readily. As in earlier studies, we observed that control of the cancer required progressively smaller doses of paclitaxel. Moreover, we found that even the lowest doses permitted by the algorithm caused continued decline in the tumor volume. In three of five MCF7 tumors and in six of seven MDA-MB-231 tumors, the tumor size fell below the treatment threshold, allowing therapy to be withdrawn, often for >8 treatment decision points, without risking rapid tumor progression (fig. S3).

Having consistently observed that tumors, once controlled, could be maintained with progressively small drug doses, even permitting withdrawal of therapy, we pursued further investigations. We hypothesized that AT strategies, by enforcing a stable tumor volume, permit relative normalization of tumor vascularity, with improved delivery of nutrients and drugs, which both reduce invasive growth and allow chemotherapy to be more effective. Furthermore, repeated application of drugs targeting proliferating cells may select for nonproliferative, noninvasive phenotypes that promote tissue-like mesenchymal organization, including relatively mature blood vessels. Other studies have, for example, demonstrated that increased tumor vascularity is associated with generally slower tumor growth (*18*).

DW imaging demonstrated that the necrotic tumor fraction in MDA-MB-231 tumors was larger in control, AT-2, and ST tumors than in AT-1. Furthermore, the necrotic fraction grew progressively smaller during AT-1 treatment so that it remained below that of untreated tumors. This was corroborated in the MCF7 tumors. Consistent with this finding, DCE MRI demonstrated increased flow and perfusion in both tumor types when treated with the AT-1 algorithm. These data were supported by subsequent histological analysis of the treated tumors at necropsy, which was consistent with the hypothesis that enforcing a stable tumor volume and regularly culling proliferating cells through

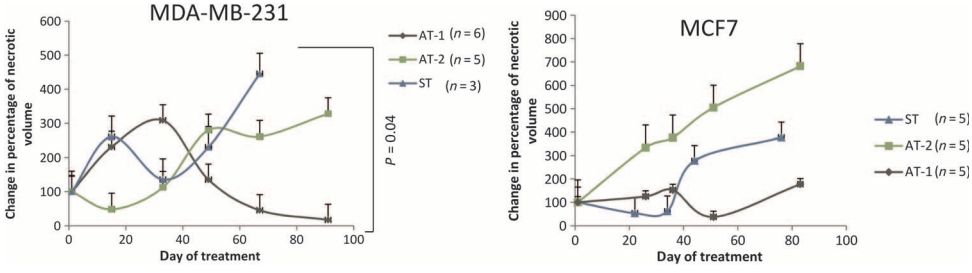

Fig. 5. Mean percentage of necrotic tissue in tumors under different treatment algorithms as determined by DW MRI. The percentages of tissue volume that is necrotic are represented relative to the first day of treatment. The data summarize results for MDA-MB-231 and MCF7, in the left and right graphs, respectively, under different therapies: standard (ST), AT-1, and AT-2. After an initial increase, the necrotic volume decreases in the AT-1 (black diamonds) cohort and increases in the ST and AT-2 cohorts. Results are means ± SE.

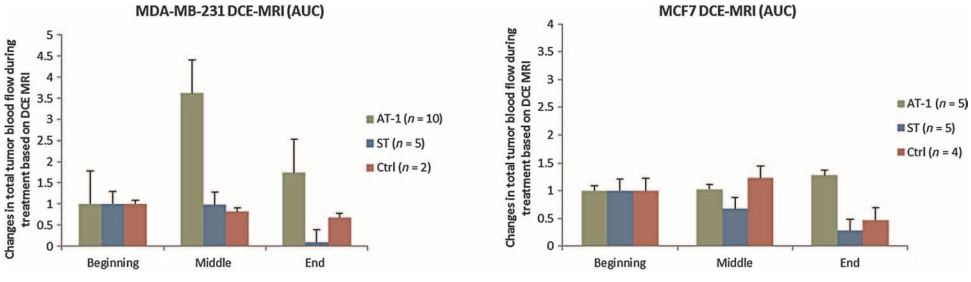

Fig. 6. Changes in tumor flow and perfusion under different treatments. Bar graphs show the changes in area under the curve (AUC) for blood flow and perfusion measurements derived from DCE MRI before (Beginning), during (Middle), and after (End) therapy relative to pretreatment baseline. In this case, only Ctrl, ST, and AT-1 therapies were monitored. The numbers in parentheses correspond to the number of mice analyzed in each group. Results are means ± SE.

Downloaded from http://stm.sciencemag.org/ at UNIVERSITY OF NORTH TEXAS on December 18, 2020

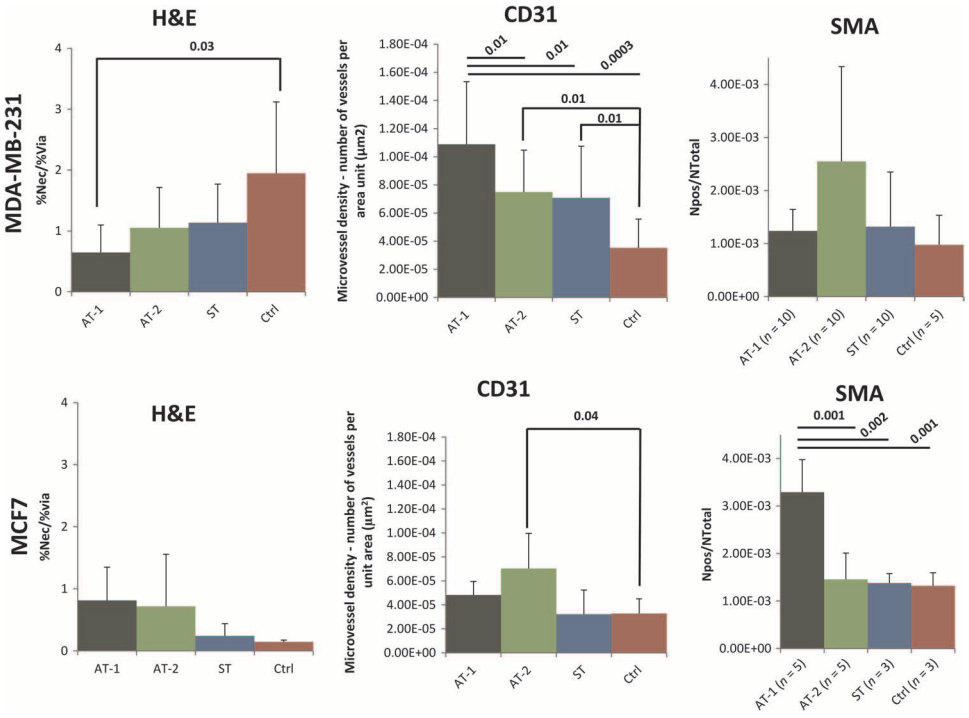

Fig. 7. Histology of tumors under different therapeutic regimens. The graphs show H&E, CD31, and SMA analysis of the indicated tumors under different therapeutic regimens, with MDA-MB-231 in the top row and MCF7 in the bottom row. Tumors treated according to AT-1 developed less necrosis (detected by H&E staining) than those on AT-2, and greater vascular density (CD31 staining) in the case of MDA-MB-231 tumors. In MCF7 tumors, necrosis did not correlate with the stability of the tumors, but increased vascular density was observed in tumors that were treated with AT-2. The AT-1 cohort had a higher microvessel density (CD31) than the Ctrl or ST groups but did not achieve statistical significance. However, the AT-1 group did have significantly higher vessel functionality demonstrated by the SMA staining. Significance testing was performed by Student's *t* test. *P* values are indicated above a line showing each comparison.

AT promote relative normalization of tumor vasculature with increased blood flow and decreased necrosis.

This increased vascular density likely increased drug delivery to the tumors and may account for the decrease in chemotherapy dose required to maintain tumor control. However, it is also possible that the frequent application of a cytotoxic drug that targets cycling cells selected for a variety of adaptive strategies. For example, it clearly selects for cells with resistance mechanisms such as up-regulation of the *MDR1* gene (*33*). However, it could also select for tumor cells that are less proliferative and, therefore, less invasive and slower-growing. Future studies will need to address this question.

Our study results have some limitations that will need to be addressed in follow-up investigations. In particular, we note that we only used two breast cancer cell lines. The total number of animals in the experiments was also relatively small, representing the smallest cohorts necessary to obtain statistically significant results, consistent with standard principles of animal experimentation. Furthermore, we were unable to unambiguously determine the intratumoral evolutionary dynamics of drug-sensitive and drug-resistant phenotypes during treatment.

In summary, we have examined a typical clinical scenario (triple-negative and ER^+ breast cancers treated with paclitaxel) and compared the response of the tumors to different treatment algorithms. We have explored a flexible treatment strategy, which varies the drug dosing and scheduling to maintain a persistent population of sensitive cells and reduce the proliferation of resistant populations. Our results suggest that this adaptive therapeutic strategy can be adapted to clinical imaging and can result in prolonged progression-free survival in breast cancer. Finally, we note that the evolutionary principles that govern AT may be applicable to a wide range of breast cancer treatments including hormonal manipulation and immunotherapy, although they will need to undergo further testing in those settings.

MATERIALS AND METHODS

Study design

The aim of this study was to design a cancer therapy on the basis of evolutionary principles. We focused our study on breast cancer, and, thus, we used ER^+ and triple-negative cell lines as preclinical models. Additional aims included fine-tuning of this evolutionary therapy and the monitoring of tumor progression by a standard radiographic technique. In all cohorts, the mice were randomly divided between treatment groups. We have replicated the experiments with mice bearing the triple-negative cell line, but not the ER^+ cell line because the latter experiment was performed to confirm that our hypothesis can apply to different breast cancer models. All data obtained for this project are shown in this manuscript, and none were excluded, even if they were outliers.

Cell culture

Bioluminescent MDA-MB-231/luc cells, which were engineered to express thermostable firefly luciferase using MDA-MB-231 human breast cancer cell (*34*) line, were cultured in RPMI 1640 medium, supplemented with 10% fetal bovine serum (FBS) (HyClone Laboratories) and 1% antibiotic-antimycotic solution (Gibco Invitrogen). Cells were selected with 100 µl of G418 per 10 ml of medium.

Fluorescent MCF7/GFP (green fluorescent protein) cells expressing pcDNA3.1(+)/zeo containing the coding region of GFP (*35*) were cultured in RPMI 1640 medium (Gibco Life Technologies), supplemented with 5% FBS (VWR Seradigm) and 1% penicillin-streptomycin solution (Gibco Life Technologies). Cells were selected with 100 µl of G418 per 10 ml of medium.

Xenograft model of human breast cancer

Orthotopic mouse xenograft experimental protocols were approved by the Institutional Animal Care and Use Committee (IACUC) at the University of South Florida. Animals were maintained and evaluated under pathogen-free conditions in accordance with IACUC standards of care at the H. Lee Moffitt Cancer Center (Tampa, FL). After detachment with 0.05% trypsin/EDTA (Corning Cellgro, Mediatech), MDA-MB-231/luc

Downloaded from http://stm.sciencemag.org/ at UNIVERSITY OF NORTH TEXAS on December 18, 2020

cells were suspended in the growth medium. The cells were washed with Dulbecco's phosphate-buffered saline (DPBS; BD Biosciences) twice and resuspended in phenol red–free 50% Matrigel (BD Biosciences) in DPBS at 1×10^8 cells/ml. The cell suspension was inoculated (~1×10^7 cells per mouse) into the mammary fat pads of 6- to 8-week-old female Nu/Nu mice (Harlan Laboratories).

For experiments with the ER^+ cell line (MCF7), 17β-estradiol 90-day release pellets, 0.72 mg per pellet (Innovative Research of America), were implanted on the dorsal region of 8-week-old female Nu/Nu mice (Harlan Laboratories) 1 day before cell injections. The cells were detached using 0.05% trypsin/EDTA (Corning, Cellgro, Mediatech) and then suspended in RPMI 1640 growth medium. The cells were washed with DPBS (Gibco Life Technologies) twice and resuspended in 50% phenol red–free Matrigel Matrix (Corning) and 50% DPBS at 2.5×10^7 cells/ml. The cell suspension was inoculated (~5×10^6 cells per mouse) into the mammary fat pads of the 8-week-old female Nu/Nu mice.

Initially, two-dimensional tumor measurements were made by calipers twice a week, and the tumor volume was calculated according to the formula: volume = π (short diameter^2) × (long diameter)/6. When the measured tumor volume exceeded 200 mm^3, we used MRI for a more accurate tumor volume monitoring until the end of experiments.

When the tumor volume reached 250 to 300 mm^3, mice were divided into three groups. Control group mice were treated with vehicle (DPBS) by intraperitoneal injections (Ctrl). The second group of mice was treated with paclitaxel (LC Laboratories) according to a standard therapy regimen, 20 mg/kg intraperitoneally, twice per week for 2.5 weeks (ST). The third group was treated with paclitaxel by AT algorithms as described below.

Adaptive therapy algorithm with dose modulation (AT-1). After an administration of the initial dose of 20 mg/kg, the subsequent treatment doses were adjusted on the basis of tumor size measured by MRI twice a week. The algorithm was similar to the AT strategy previously reported (*8*). Drug dose was reduced by 50% of the previously applied dose if the tumor volume decreased by 20% or more from the previous volume. However, we increased the drug dose by 50% of the previous dose if tumor size increased by 20% or more with respect to previous size, with a maximum dose of 20 mg/kg of paclitaxel in a single treatment. We repeated the same dose if the tumor size was within the range of ±20% of the previous volume. We set up a minimum tumor volume cutoff of 150 mm^3, below which paclitaxel treatment was skipped until the tumor size increased again.

Adaptive therapy algorithm with treatment skipping (AT-2). Starting with a moderate-high dose of paclitaxel (15 mg/kg), the subsequent drug treatment was determined on the basis of the percentage of tumor growth rate measured twice a week. If the tumor volume (T_n) was increased by ≥25% compared to two volume measurements before (T_{n-2}), a fixed dose (15 mg/kg) of paclitaxel was administered. The treatment was skipped if the tumor volume remained constant or reduced with respect to the two previous measurements. No minimum cutoff was applied.

MRI analysis

Magnetic resonance data were acquired with a 7-T horizontal magnet Agilent ASR 310 (Agilent Technologies Inc.) equipped with nested 205/120/HDS gradient insert and a bore size of 310 mm. Before imaging, the animals were placed in an induction chamber and anesthetized with 2% isoflurane delivered in 1.5 liter/min oxygen ventilation. Upon complete induction, animals were restrained in a custom-designed holder and inserted into the magnet while constantly receiving isoflurane. Body temperature (36° ± 1°C) and respiratory function were monitored continuously (SAII System). A 35-mm Litzcage coil (Doty Scientific) was used to carry out axial T_2-weighted fast spin-echo multislice experiments [acquired with TE/TR (echo time/repetition time) = 72 ms/1000 ms, field of view (FOV) = 35 × 35 mm^2, matrix = 128 × 128, yielding a spatial in-plane resolution of 273 μm, slice thickness of 1.5 mm, and three averages]. Applying the same axial slice plane, a DW sequence was also acquired using three *b* values (50, 500, and 1000 s/m^2) and TE/TR of 36/1325 ms. The total acquisition time was always less than 15 min. Images were reconstructed with VnmrJ software (Agilent Technologies Inc.). Tumor volumes were obtained from the high-resolution T_2-weighted data sets and measured by manually drawn regions of interest (ROIs) encompassing the entire tumors.

We used an in-house MATLAB program (available upon request) to obtain volumetric information from the T_2-weighted images. The ADC analysis was performed by nonlinear least-squares regression with tumor ADC values calculated by the following equation: $S(b) = S(0)\exp(-\mathrm{ADC}^*b)$, where *b* is the diffusion-sensitizing factor, $S(b)$ is the signal intensity as a function of diffusion weighting, and $S(0)$ is the non-DW intensity (*15*).

DCE MRI experiments were carried out in the same spectrometer using a T_1 gradient echo multislice experiment (acquired with TE/TR = 4/117 ms). FOV and in-plane geometry were the same as in the T_2 experiments. In this case, we took only the six slices in the middle of the tumors. Imaging started 1 min after injection of contrast agent (Magnevist, 0.1 mmol/kg) and continued for 20 min. The experiments were analyzed with AEDES (*35*) software.

Histological analysis

MDA-MB-231 and MCF7 tumor samples were collected at the completion of the experiment in the case of tumors with controlled growth, or when tumors reached a volume of 2000 mm^3. After collection, the tumors were processed by soaking in formalin for at least 24 hours and then embedded in paraffin blocks. Sequential slices of each tumor were collected for processing with H&E (Abcam) and vascularity (CD31 and SMA, Abcam) staining. The slices were imaged at the Moffitt Cancer Center microscope core facilities, using an Aperio ScanScope XT microscope and Aperio Spectrum version 10.2.5.2352 image analytic software (Leica Biosystems Inc.). To optimize image analysis of the IHC slices, we trained the algorithm by using ROIs that were selected manually to represent ROIs that are positive and negative for each stain. After this process, the software developed an algorithm that was used to analyze the slices. After initial algorithm training, the software developed a final algorithm, which was used to automatically analyze the slides with a pixel resolution.

Statistical analysis

For volume and necrosis data, an analysis of variance (ANOVA) test was performed to evaluate for differences in tumor growth between AT-1 and AT-2. For analysis of histology data, we used a *t* test with one tail and unequal variance.

SUPPLEMENTARY MATERIALS

www.sciencetranslationalmedicine.org/cgi/content/full/8/327/327ra24/DC1

Fig. S1. Individual volumetric graphics of all mice used in this work.

Fig. S2. Total dose of paclitaxel delivered in each mouse.

Fig. S3. Bar graphs showing paclitaxel doses skipped for all mice under AT-1 therapy.

Downloaded from http://stm.sciencemag.org/ at UNIVERSITY OF NORTH TEXAS on December 18, 2020

Table S1. Total dose of paclitaxel and change in weight of mice in MDA-MB-231 batches A and B (provided in Excel format).
Table S2. Total dose of paclitaxel and change in weight of mice in MDA-MB-231 batch C (provided in Excel format).
Table S3. Total dose of paclitaxel and change in weight of mice in MDA-MB-231 batch D (provided in Excel format).
Table S4. Total dose of paclitaxel and change in weight of mice with MCF7 tumors (provided in Excel format).

REFERENCES AND NOTES

1. M. S. U. Hassan, J. Ansari, D. Spooner, S. A. Hussain, Chemotherapy for breast cancer (Review). *Oncol. Rep.* **24**, 1121–1131 (2010).
2. N. U. Lin, R. Gelman, E. P. Winer, Dose density in breast cancer: A simple message? *J. Natl. Cancer Inst.* **97**, 1712–1714 (2005).
3. E. Frei III, A. Elias, C. Wheeler, P. Richardson, W. Hryniuk, The relationship between high-dose treatment and combination chemotherapy: The concept of summation dose intensity. *Clin. Cancer Res.* **4**, 2027–2037 (1998).
4. A. D. Seidman, Current status of dose-dense chemotherapy for breast cancer. *Cancer Chemother. Pharmacol.* **56** (Suppl. 1), 78–83 (2005).
5. L. Norton, R. Simon, The Norton-Simon hypothesis revisited. *Cancer Treat. Rep.* **70**, 163–169 (1986).
6. R. S. Mehta, D. Jackson, T. Schubbert, Metronomic schedule of paclitaxel is effective in hormone receptor–positive and hormone receptor–negative breast cancer. *J. Clin. Oncol.* **27**, 3067–3068 (2009).
7. E. Montagna, G. Cancello, S. Dellapasqua, E. Munzone, M. Colleoni, Metronomic therapy and breast cancer: A systematic review. *Cancer Treat. Rev.* **40**, 942–950 (2014).
8. G. Bouche, N. André, S. Banavali, F. Berthold, A. Berruti, G. Bocci, G. Brandi, U. Cavallaro, S. Cinieri, M. Colleoni, G. Curigliano, T. Di Desidero, A. Eniu, N. Fazio, R. Kerbel, L. Hutchinson, U. Ledzewicz, E. Munzone, E. Pasquier, O. G. Scharovsky, Y. Shaked, J. Stěrba, M. Villalba, F. Bertolini, Lessons from the Fourth Metronomic and Anti-angiogenic Therapy Meeting, 24–25 June 2014, Milan. *Ecancermedicalscience* **8**, 463 (2014).
9. R. A. Gatenby, A change of strategy in the war on cancer. *Nature* **459**, 508–509 (2009).
10. A. S. Silva, Y. Kam, Z. P. Khin, S. E. Minton, R. J. Gillies, R. A. Gatenby, Evolutionary approaches to prolong progression-free survival in breast cancer. *Cancer Res.* **72**, 6362–6370 (2012).
11. M. Gerlinger, C. Swanton, How Darwinian models inform therapeutic failure initiated by clonal heterogeneity in cancer medicine. *Br. J. Cancer* **103**, 1139–1143 (2010).
12. R. J. Gillies, C. I. Flowers, J. S. Drukteinis, R. A. Gatenby, A unifying theory of carcinogenesis, and why targeted therapy doesn't work. *Eur. J. Radiol.* **81** (Suppl. 1), S48–S50 (2012).
13. M. M. Gottesman, T. Fojo, S. E. Bates, Multidrug resistance in cancer: Role of ATP–dependent transporters. *Nat. Rev. Cancer* **2**, 48–58 (2002).
14. R. A. Gatenby, J. J. Cunningham, J. S. Brown, Evolutionary triage governs fitness in driver and passenger mutations and suggests targeting never mutations. *Nat. Commun.* **5**, 5499 (2014).
15. R. A. Gatenby, R. J. Gillies, A microenvironmental model of carcinogenesis. *Nat. Rev. Cancer* **8**, 56–61 (2008).
16. H. J. Broxterman, H. J. Broxterman, H. M. Pinedo, C. M. Kuiper, L. C. Kaptein, G. J. Schuurhuis, J. Lankelma, Induction by verapamil of a rapid increase in ATP consumption in multidrug-resistant tumor cells. *FASEB J.* **2**, 2278–2282 (1988).
17. F. Shen, S. Chu, A. K. Bence, B. Bailey, X. Xue, P. A. Erickson, M. H. Montrose, W. T. Beck, L. C. Erickson, Quantitation of doxorubicin uptake, efflux, and modulation of multidrug resistance (MDR) in MDR human cancer cells. *J. Pharmacol. Exp. Ther.* **324**, 95–102 (2008).
18. S. Adkins, A. Shabbir, Biology, ecology and management of the invasive parthenium weed (*Parthenium hysterophorus* L.). *Pest Manag. Sci.* **70**, 1023–1029 (2014).
19. B. W. Alto, R. L. Lampman, B. Kesavaraju, E. J. Muturi, Pesticide-induced release from competition among competing *Aedes aegypti* and *Aedes albopictus* (Diptera: Culicidae). *J. Med. Entomol.* **50**, 1240–1249 (2013).
20. D. Basanta, R. A. Gatenby, A. R. A. Anderson, Exploiting evolution to treat drug resistance: Combination therapy and the double bind. *Mol. Pharm.* **9**, 914–921 (2012).
21. Y. Kam, T. Das, S. Minton, R. A. Gatenby, Evolutionary strategy for systemic therapy of metastatic breast cancer: Balancing response with suppression of resistance. *Womens Health* **10**, 423–430 (2014).
22. P. A. Orlando, R. A. Gatenby, J. S. Brown, Cancer treatment as a game: Integrating evolutionary game theory into the optimal control of chemotherapy. *Phys. Biol.* **9**, 065007 (2012).
23. R. A. Gatenby, A. S. Silva, R. J. Gillies, B. R. Frieden, Adaptive therapy. *Cancer Res.* **69**, 4894–4903 (2009).
24. R. K. Jain, Normalization of tumor vasculature: An emerging concept in antiangiogenic therapy. *Science* **307**, 58–62 (2005).
25. S. Ueda, I. Kuji, T. Shigekawa, H. Takeuchi, H. Sano, E. Hirokawa, H. Shimada, H. Suzuki, M. Oda, A. Osaki, T. Saeki, Optical imaging for monitoring tumor oxygenation response after initiation of single-agent bevacizumab followed by cytotoxic chemotherapy in breast cancer patients. *PLOS One* **9**, e98715 (2014).
26. S. Goel, A. H.-K. Wong, R. K. Jain, Vascular normalization as a therapeutic strategy for malignant and nonmalignant disease. *Cold Spring Harb. Perspect. Med.* **2**, a006486 (2012).
27. S. M. Kakkad, M.-F. Penet, A. Akhbardeh, A. P. Pathak, M. Solaiyappan, V. Raman, D. Leibfritz, K. Glunde, Z. M. Bhujwalla, Hypoxic tumor environments exhibit disrupted collagen I fibers and low macromolecular transport. *PLOS One* **8**, e81869 (2013).
28. M. McDermott, A. J. Eustace, S. Busschots, L. Breen, J. Crown, M. Clynes, N. O'Donovan, B. Stordal, In vitro development of chemotherapy and targeted therapy drug-resistant cancer cell lines: A practical guide with case studies. *Front. Oncol.* **4**, 40 (2014).
29. B. Györffy, V. Serra, K. Jürchott, R. Abdul-Ghani, M. Garber, U. Stein, I. Petersen, H. Lage, M. Dietel, R. Schäfer, Prediction of doxorubicin sensitivity in breast tumors based on gene expression profiles of drug-resistant cell lines correlates with patient survival. *Oncogene* **24**, 7542–7551 (2005).
30. M. Greaves, C. C. Maley, Clonal evolution in cancer. *Nature* **481**, 306–313 (2012).
31. K. Seibert, S. M. Shafie, T. J. Triche, J. J. Whang-Peng, S. J. O'Brien, J. H. Toney, K. K. HUff, M. E. Lippman, Clonal variation of MCF-7 breast cancer cells in vitro and in athymic nude mice. *Cancer Res.* **43**, 2223–2239 (1983).
32. B. Tegze, Z. Szállási, I. Haltrich, Z. Pénzváltó, Z. Tóth, I. Likó, B. Győrffy, Parallel evolution under chemotherapy pressure in 29 breast cancer cell lines results in dissimilar mechanisms of resistance. *PLOS One* **7**, e30804 (2012).
33. B. Baggett, R. Roy, S. Momen, S. Morgan, L. Tisi, D. Morse, R. J. Gillies, Thermostability of firefly luciferases affects efficiency of detection by in vivo bioluminescence. *Mol. Imaging* **3**, 324–332 (2004).
34. L. Liu, G. Duclos, B. Sun, J. Lee, A. Wu, Y. Kam, E. D. Sontag, H. A. Stone, J. C. Sturm, R. A. Gatenby, R. H. Austin, Minimization of thermodynamic costs in cancer cell invasion. *Proc. Natl. Acad. Sci. U.S.A.* **110**, 1686–1691 (2013).
35. http://aedes.uef.fi/

Funding: This work was supported by the James S. McDonnell Foundation grant, "Cancer therapy: Perturbing a complex adaptive system," NIH/National Cancer Institute (NCI) R01CA170595, Application of Evolutionary Principles to Maintain Cancer Control (PQ21), and NIH/NCI U54CA143970-05 [Physical Science Oncology Network (PSON)] "Cancer as a complex adaptive system." This work has been supported in part by the Analytic Microscopy Core Facility at the H. Lee Moffitt Cancer Center and Research Institute, an NCI-designated Comprehensive Cancer Center (P30-CA076292). **Author contributions:** Designed experiments: R.A.G., R.J.G., P.M.E.-N., Y.K., and A.S. Performed experiments: P.M.E.-N., Y.K., T.D., P.F., E.R., S.H., and G.M. Wrote the manuscript: P.M.E.-N., Y.K., S.M., R.J.G., and R.A.G. **Competing interests:** R.J.G. is a member of the scientific advisory board and an investor in HealthMyne Inc., a radiology PACS company (no relation to the current manuscript). The authors declare that they have no competing interests.

Submitted 31 October 2015
Accepted 14 January 2016
Published 24 February 2016
10.1126/scitranslmed.aad7842

Citation: P. M. Enriquez-Navas, Y. Kam, T. Das, S. Hassan, A. Silva, P. Foroutan, E. Ruiz, G. Martinez, S. Minton, R. J. Gillies, R. A. Gatenby, Exploiting evolutionary principles to prolong tumor control in preclinical models of breast cancer. *Sci. Transl. Med.* **8**, 327ra24 (2016).

Downloaded from http://stm.sciencemag.org/ at UNIVERSITY OF NORTH TEXAS on December 18, 2020

Science Translational Medicine

Exploiting evolutionary principles to prolong tumor control in preclinical models of breast cancer

Pedro M. Enriquez-Navas, Yoonseok Kam, Tuhin Das, Sabrina Hassan, Ariosto Silva, Parastou Foroutan, Epifanio Ruiz, Gary Martinez, Susan Minton, Robert J. Gillies and Robert A. Gatenby

Sci Transl Med **8**, 327ra24327ra24.
DOI: 10.1126/scitranslmed.aad7842

Evolution of cancer therapy

The standard approach to treating cancer is giving patients the maximum tolerated amount of chemotherapy with the goal of doing the maximum possible damage to the tumor without killing the patient. This method is relatively effective, but it also causes major toxicities. Now, Enriquez-Navas *et al.* have demonstrated a different approach for ensuring efficacy of chemotherapy and minimizing toxicity. The authors used an evolutionary approach, where the dose of chemotherapy is guided by the tumor's response to the previous dose, allowing a gradual withdrawal of the drug if the tumor continues to respond. This method proved quite effective for paclitaxel treatment in two different mouse models and warrants further evaluation in additional models as well as human trials.

ARTICLE TOOLS http://stm.sciencemag.org/content/8/327/327ra24

SUPPLEMENTARY MATERIALS http://stm.sciencemag.org/content/suppl/2016/02/22/8.327.327ra24.DC1

RELATED CONTENT
http://stm.sciencemag.org/content/scitransmed/3/90/90ra59.full
http://stm.sciencemag.org/content/scitransmed/7/318/318ra202.full
http://stm.sciencemag.org/content/scitransmed/7/313/313ra182.full
http://stm.sciencemag.org/content/scitransmed/7/315/315ra188.full
http://stm.sciencemag.org/content/scitransmed/8/327/327fs5.full
http://stm.sciencemag.org/content/scitransmed/8/334/334ra53.full
http://science.sciencemag.org/content/sci/355/6330/1144.full
http://science.sciencemag.org/content/sci/351/6278/1204.full
http://stm.sciencemag.org/content/scitransmed/11/488/eaav0936.full
http://science.sciencemag.org/content/sci/368/6495/1127.full

REFERENCES This article cites 34 articles, 9 of which you can access for free
http://stm.sciencemag.org/content/8/327/327ra24#BIBL

PERMISSIONS http://www.sciencemag.org/help/reprints-and-permissions

Use of this article is subject to the Terms of Service

Science Translational Medicine (ISSN 1946-6242) is published by the American Association for the Advancement of Science, 1200 New York Avenue NW, Washington, DC 20005. The title *Science Translational Medicine* is a registered trademark of AAAS.

Copyright © 2016, American Association for the Advancement of Science

Downloaded from http://stm.sciencemag.org/ at UNIVERSITY OF NORTH TEXAS on December 18, 2020